Analytical and Bioanalytical Chemistry (2024) 416:4249–4260
https://doi.org/10.1007/s00216-024-05362-1

RESEARCH PAPER

Factors affecting protein recovery during Hsp40 affinity profiling

Maureen R. Montoya[1] · Guy M. Quanrud[1] · Liangyong Mei[2] · José L. Moñtano[1] · Caleb Hong[1] · Joseph C. Genereux[1]

Received: 9 October 2023 / Revised: 30 April 2024 / Accepted: 22 May 2024 / Published online: 8 June 2024

Abstract

The identification and quantification of misfolded proteins from complex mixtures is important for biological characterization and disease diagnosis, but remains a major bioanalytical challenge. We have developed Hsp40 Affinity Profiling as a bioanalytical approach to profile protein stability in response to cellular stress. In this assay, we ectopically introduce the Hsp40 ^{Flag}DNAJB8^{H31Q} into cells and use quantitative proteomics to determine how protein affinity for DNAJB8 changes in the presence of cellular stress, without regard for native clients. Herein, we evaluate potential approaches to improve the performance of this bioanalytical assay. We find that although intracellular crosslinking increases recovery of protein interactors, this is not enough to overcome the relative drop in DNAJB8 recovery. While the J-domain promotes Hsp70 association, it does not affect the yield of protein association with DNAJB8 under *basal* conditions. By contrast, crosslinking and J-domain ablation both substantially increase relative protein interactor recovery with the structurally distinct Class B Hsp40 DNAJB1 but are completely compensated by poorer yield of DNAJB1 itself. Cellular thermal stress promotes increased affinity between DNAJB8^{H31Q} and interacting proteins, as expected for interactions driven by recognition of misfolded proteins. DNAJB8^{WT} does not demonstrate such a property, suggesting that under stress misfolded proteins are handed off to Hsp70. Hence, we find that DNAJB8^{H31Q} is still our most effective recognition element for the recovery of destabilized client proteins following cellular stress.

Keywords Hsp40 · DNAJB1 · DNAJB8 · AP-MS · Misfolded proteins · Proteomics

Introduction

Cellular health requires the maintenance of protein homeostasis to prevent the accumulation of misfolded proteins and proteotoxic species [1]. There are many stressors that can threaten this homeostasis, including environmental exposure, aging, and genetic mutations [2]. Although understanding the role of protein misfolding in health and disease is a central question in cellular biology, there are few bioanalytical techniques for identifying misfolded proteins in the cell. Powerful structural biology techniques such as chemical footprinting and limited proteolysis can be used to identify conformational changes in proteins, but the increased chemical complexity can challenge sampling the proteome [3–9]. Alternatively, recognition by a chaperone can be used as a proxy for protein stability [10, 11]. Based on this principle, we have developed Hsp40 Affinity Profiling as a bioanalytical technique to assess misfolded proteins [12–14]. This approach exploits the capacity of Hsp40 family proteins (also called J-domain proteins) to recognize and bind to misfolded proteins [15, 16]. In this assay, the human Hsp40 DNAJB8 is expressed in cells prior to challenging the cells with the toxicant of interest. Misfolded proteins accumulate on DNAJB8, so that after lysis, they can be co-purified and identified and quantified by quantitative mass spectrometry (Fig. 1). A J-domain mutation, H31Q, was introduced into DNAJB8 to prevent handoff of misfolded proteins to Hsp70 and thus ensure accumulation on DNAJB8 [17, 18]. The strong affinity of DNAJB8^{H31Q} for misfolded proteins allows stringent washing with RIPA buffer to remove non-specific interactors. This approach has enabled us to identify proteins that are sensitive to metals and to electrophilic herbicides.

✉ Joseph C. Genereux
josephg@ucr.edu

[1] Department of Chemistry, University of California, 501 Big Springs Rd, Riverside, CA 92521, USA

[2] Department of Chemistry, University of North Florida, Jacksonville, FL, USA

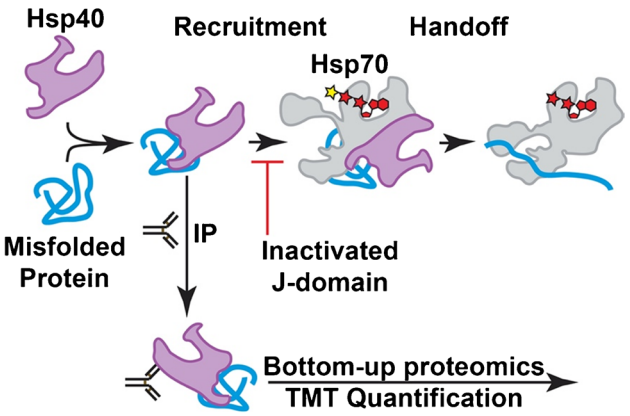

Fig. 1 Hsp40 proteins recruit misfolded proteins to Hsp70 in a manner dependent on their J-domain. We exploit this by using DNAJB8 to recognize misfolded proteins, which can then be extracted with immunoprecipitation and quantified by quantitative mass spectrometry-based proteomics

Although our approach has been validated by its success, we have not established answers to key questions. Firstly, it is not clear that DNAJB8 is the only Hsp40 that could be used in this assay. Other Hsp40s might be able to be used to extract and assess the same misfolded proteins from biological samples or perhaps even to target a complementary proteome. Secondly, although the H31Q mutation in the J-domain was introduced to avoid handoff of misfolded proteins to Hsp70, we do not know if it is necessary. Finally, we have not fully evaluated whether crosslinking in the cell provides improved misfolded protein recovery. Herein, we consider these questions, finding that DNAJB8 requires neither crosslinking nor mutation to pull down its distinct proteome. However, under heat stress, the H31Q mutation is necessary to observe increased Hsp40 affinity.

Materials and methods

Reagents Biochemical reagents and buffer components were purchased from Fisher Scientific, VWR, or Millipore Sigma. Millipore water and sterilized consumables were used for all biochemical experiments.

Molecular cloning DNAJB1 was amplified from cDNA derived from HEK293T cells (ATCC) using TRIzol (Thermo Fisher Scientific) and inserted into the pFlag.CMV2 vector by PIPE cloning [19] using Q5 polymerase and the primers:

5′-CAGATCTATCGATGAATTCGCTATTGGAAGAAC CTGCTCAAG-3′, 5′-CTTGAGCAGGTTCTTCCAATA GCGAATTCATCGATAGATCTG-3′, 5′-GTAGTAGTC TTTACCCATGACCTTGTCGTCATCGTCTTTG-3′, and 5′-CAAAGACGATGACGACAAGGTCATGGGTAAAGA CTACTAC-3′. The H32Q mutation was introduced into DNAJB1 using site-directed mutagenesis with the oligonucleotides 5′-CTACCAACCGGACAAGAACAAGGAGCC CGG-3′ and 5′-CCGGTTGGTAGCGCAGCGCC-3′. ^{Flag}DNAJB8^{WT}.CMV2, ^{Flag}DNAJB8^{H31Q}.CMV2, and EGFP. pDest30 have been reported [20, 21]. Constructs were analytically digested and sequenced (Retrogen) to confirm identity. All cloning enzymes and buffers were purchased from New England Biolabs and primers were purchased from IDT.

Human tissue culture These experiments were performed in HEK293T cells, which do not represent any specific human tissue type. However, proteostasis mechanisms tend to be highly conserved across euploidal cell lines. Therefore, it is likely that the general observations made here will hold, although specific clients might be handled differently. HEK293T cells were cultured in DMEM (Corning) supplemented with 10% fetal bovine serum (FBS, Seradigm), 2 mM L-glutamine (Corning), and penicillin–streptomycin (100 IU/mL,100 µg/mL, Corning). Cells were transfected with plasmid DNA by the calcium phosphate method. Every experiment involving DNAJB8 used one 10 cm plate per condition. 4-plex experiments involving DNAJB1 used two 10 cm plates per condition to account for its lower overexpression. Where heat shock was applied, cells were placed in an incubator at the indicated temperature for 30 min and then immediately harvested, washed, and the pellets frozen at –80 °C.

Immunoprecipitation Cells were harvested from confluent dishes at 36 h to 48 h post-transfection. If crosslinking was used, cells were incubated in the indicated concentration of freshly prepared dithiobis succinimidyl propionate (DSP) in 1% DMSO/PBS for 30 min with rotation at ambient temperature and then quenched by addition of Tris pH 8.0 (to 90 mM final concentration) and rotation for 15 min. After crosslinking, or directly after harvest for experiments without crosslinking, cells were lysed for 30 min on ice in lysis buffer supplemented with fresh 1 × protease inhibitor cocktail (Roche). Unless otherwise indicated, lysis was performed in RIPA buffer (150 mM NaCl, 50 mM Tris pH 7.5, 1% Triton X-100, 0.5% sodium deoxycholate, 0.1% SDS). For low stringency experiments using DNAJB1, lysis was performed with 0.1% Triton X-100 in TBS (10 mM Tris pH 7.5, 150 mM NaCl). Lysate was separated from cell debris by centrifugation at 21,100 × g for 15 min at 4 °C. Protein was quantified by Bradford assay (Bio-Rad). Lysates were precleared with 15 µL sepharose-4B beads (Millipore Sigma) for 30 min at 4 °C, followed by immunoprecipitation with 15 µL M2 anti-FLAG Magnetic Beads (Millipore Sigma) and overnight rotation at 4 °C. Beads were washed four times with lysis buffer the next day for DNAJB8 or 3 days later for DNAJB1. Proteins were eluted from the beads by boiling in 30 µL of Laemmli concentrate (120 mM Tris pH 6.8, 60%

glycerol, 12% SDS, brilliant phenol blue to color). About 17% of each eluate was reserved for silver stain analysis, and the remainder prepared for mass spectrometry.

Silver stain Eluates were boiled for 5 min at 100 °C with 0.17 M DTT, loaded into 1.0 mm, 12% polyacrylamide gels, and separated by SDS-PAGE. Gels were rinsed in Millipore water for 5 min. Gels were left overnight in fixing solution (10% acetic acid, 30% ethanol), washed 3 × 20 min in 35% ethanol, sensitized (0.02% sodium thiosulfate) for 2 min, washed with Millipore water 3 × 2 min, and stained for 30 min to overnight in Ag staining solution (0.2% $AgNO_3$, 0.076% formalin). Gels were washed 2 × 1 min with Millipore water and developed (6% sodium carbonate, 0.05% formalin, 0.0004% sodium thiosulfate) until bands reached desired intensity and imaged on a white-light transilluminator (UVP).

TMT-MuDPIT Immunoprecipitates were prepared for TMT-AP-MS according to standard protocols [22–24]. After TMT labeling, each TMT reaction was quenched with 0.4% ammonium bicarbonate. Labeled digests were combined and fractionated by SCX in line with a reversed-phase analytical column to enable two-dimensional separation prior to electrospray ionization. Peptides were analyzed using a LTQ Orbitrap Velos Pro in data-dependent mode. The top ten peaks from each full precursor scan were fragmented by HCD (stepped collision energies of 36%, 42%, 48% with 100 ms activation time) to acquire fragmentation spectra with 7500 resolving power at 400 m/z. Dynamic exclusion parameters were 1 repeat count, 30 ms repeat duration, 500 exclusion list size, 120 s exclusion duration, and 2.00 Da exclusion width. Peptide-spectra matches were evaluated by FragPipe [25] against the Uniprot human proteome database (Jun 11, 2021 release, longest entry for each protein) with 20,429 sequences (including common contaminants) plus a full reversed sequence decoy set. Cysteine alkylation (+57.02146 Da) and TMT modification (+229.1629 on lysine and N-termini) were set as fixed modifications. DSP (+145.0198 Da) was not included as a variable modification on lysine, as in our experience recovery of DSP modified peptides is similar to the estimated identification false discovery rate, leading to poor confidence in those identifications. Half tryptic and fully tryptic peptides were allowed, as were 2 missed cleavages per peptide. A mass tolerance of 1 Da for precursors and 20 ppm for fragments was allowed to ensure adequate sampling of decoy proteins [26]. Decoy proteins, non-human contaminants, immunoglobulins, and keratins were filtered from the final protein list.

Gene ontology Selective interactors were analyzed by Panther 17.0 by comparison to all *Homo sapiens* genes by biological process. Ontologies were evaluated by false discovery rate based on Fisher's exact test.

Statistical methods TMT intensity ratios were analyzed using Excel. Box and whisker plots are presented with lines marking median values, X marking average values, boxes from the first to third quartiles, whiskers extending to minimum and maximum values (excluding outliers), and outliers defined at points greater than 1.5-fold the interquartile range beyond the first and third quartiles. Violin plots were generated in R using the ggplot2 library. For bait vs. mock experiments, Pearson's R-derived t-statistics were used for determination of *p*-values [20]. *q*-values (q_{BH}) were determined from *p*-values using Storey's modification of Benjamini-Hochberg's methodology [27, 28] and adjusted to maintain monotonicity. For heat shock experiments with $DNAJB8^{H31Q}$ and $DNAJB8^{WT}$, integrated TMT reporter ion intensities of identified proteins were normalized to bait intensities.

Results

$^{Flag}DNAJB8^{WT}$ specifically enriches hundreds of proteins in TMT-AP-MS

We originally incorporated the J-domain H31Q mutation into DNAJB8 to prevent hand-off of mutant proteins to Hsp70 (Fig. 1), but we did not evaluate whether this mutation was necessary for the observed strong protein binding [12]. To evaluate whether $DNAJB8^{WT}$ has similarly strong association with proteins from cellular lysates, we overexpressed $^{Flag}DNAJB8^{WT}$ or mock (eGFP) in HEK293T cells, lysed, and immunoprecipitated using the M2 anti-Flag antibody crosslinked to magnetic beads (Fig. 2A and Figure S1). To minimize non-specific interactions, beads were washed well with RIPA buffer. This high detergent solution (150 mM NaCl, 50 mM Tris pH 7.5, 1% Triton X-100, 0.5% sodium deoxycholate, 0.1% SDS) was originally developed to break up weak or non-specific protein–protein interactions. Tryptic digests of the eluate were isobarically labeled with TMT tags, quantified by MuDPIT LC–MS, and relative protein abundances inferred from TMT reporter ion ratios for identified peptides. Interaction significance was determined using our previously reported bait correlation method [20].

We identified 2743 proteins across the three runs, with 2623 showing preferential recovery (q-value < 0.01) in the presence of DNAJB8 (Fig. 2B and Table S1). These proteins are highly enriched in RNA binding proteins (705 identified out of 1689 annotated, GO:0003723). Proteins that are selective for the *absence* of DNAJB8 include KIF11, WDR77, and PRMT5, which are well-characterized binders to anti-Flag antibodies and are prominent in control Flag immunoprecipitations in the CRAPome database [29, 30]. Presumably, these proteins bind to anti-Flag antibodies that are not bound to Flag-containing protein. Piette et al. recently

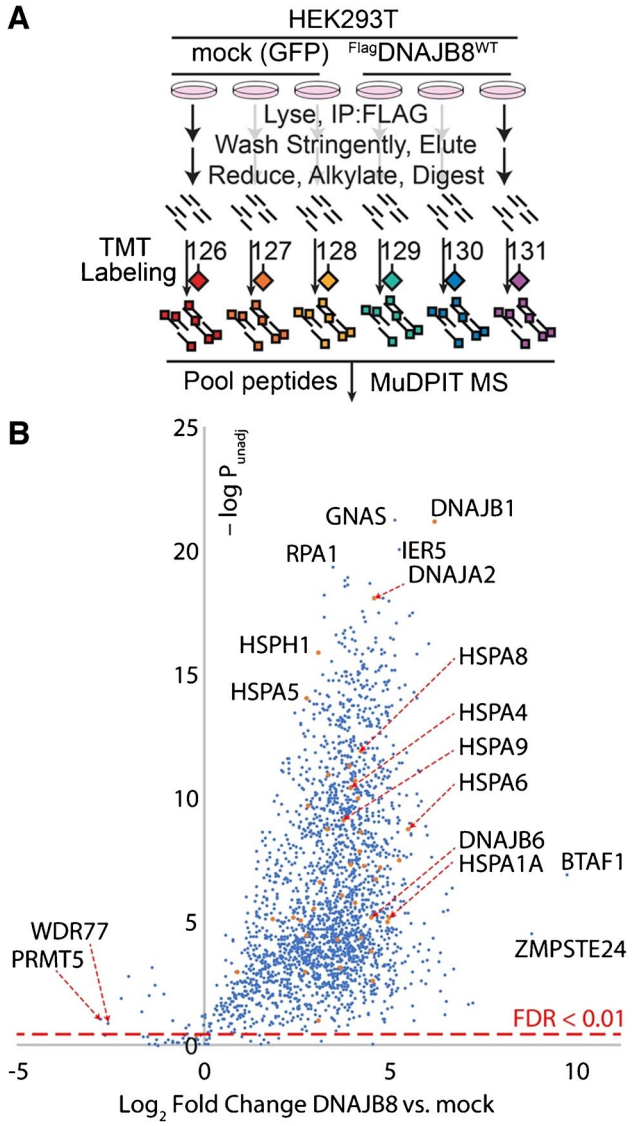

Fig. 2 **A** Experimental design to identify strong ^{Flag}DNAJB8^{WT} interactors from HEK293T cellular lysates. Nine biological replicates, comprising three LC–MS runs, were performed. **B** Volcano plot of proteins recovered from ^{Flag}DNAJB8^{WT} immunoprecipitates. The global false discovery rate for all proteins, using Storey's modification of Benjamini–Hochberg analysis, is 2.6%. The dashed red line on the chart shows the 1% FDR cut-off. 60 proteins that were not quantified in any mock replicate are not shown

reported a careful identification of human Hsp40 interactors in the cell based on AP-MS experiments and global comparison to controls [31]. They found 34 high-confidence DNAJB8 interactors, of which we identify 30 in our assay. It is important to note that their study was designed to discover specific *native interactors* of all human Hsp40s; by contrast, our assay does not require that DNAJB8 affinity only be determined for bona fide clients of the co-chaperone and we make no efforts to discriminate between native clients and the rest of the proteome. DNAJB8 co-immunoprecipitates several cytosolic Hsp70-associated proteins, including constitutive cytosolic Hsp70 HSPA8, the inducible cytosolic Hsp70s HSPA1A and HSPA6, and cytosolic Hsp70 co-chaperones STUB1, HSPA4, DNAJB1, DNAJB6, and DNAJA2. These strong associations are consistent with the canonical role of Hsp40 proteins as co-chaperones of Hsp70. In addition, the ER Hsp70 HSPA5 and mitochondrial Hsp70 HSPA9 were also recovered (alongside 183 and 112 other mitochondrial and ER proteins, respectively). While mitochondrial and ER pre-proteins can interact with cytosolic chaperones prior to their trafficking or during degradation, it is likely that these associations are taking place post-lytically and do not represent *native* clients in the cell. In the context of an assay for misfolded protein, however, post-lytic interactions serve to expand the profiling space. The large number of proteins that co-purify with DNAJB8^{WT} indicate that J-domain ablation is not necessary for the strong protein binding properties of DNAJB8.

Influence of crosslinking and J-domain inactivation on DNAJB8 client binding

Our previous interacting protein analysis for DNAJB8^{H31Q}, in the presence of the cell-penetrable crosslinker DSP, found 463 interacting proteins (using the criteria that $p < 0.05$, fold change > 1.2 vs. mock; 476 with $q < 0.01$) [20]. Of these, 251 are shared with DNAJB8^{WT} using the same criteria, while 2183 protein groups were high-confidence interactors with DNAJB8^{WT} without crosslinking but not DNAJB8^{H31Q} with crosslinking. To better understand the role of crosslinking and J-domain inactivation in DNAJB8 interactor recovery, we performed a series of TMT-AP-MS experiments directly comparing four conditions: WT vs. H31Q, and ± crosslinker (Fig. 3A and Figure S2A). For these experiments, we used the reversible crosslinker DSP. DSP is cell-penetrable and allows us to immortalize cellular interactions prior to lysis [32]. After immunoprecipitation and elution, we reverse the crosslinks with TCEP to allow peptide identification during mass spectrometry. Because crosslink yield tends to be low on a per peptide basis, we do not include DSP modification as a variable modification for peptide-spectral matching. An initial optimization found that protein recovery closely tracked DNAJB8 levels regardless of crosslinker concentration (Figure S2B,C), so we went forward with 1 mM as the same concentration that we previously used [20]. We confirmed that DNAJB8^{WT} and DNAJB8^{H31Q} have similar expression and immunoprecipitation efficiencies (Fig. 3B and Figure S2D, E). We expected that J-domain mutation would decrease interactions with Hsp70s and indirectly decrease interactions with Hsp70 co-chaperones, while crosslinking would increase the recovery of most protein interactors by preventing their dissociation during lysis and washing of the beads with RIPA.

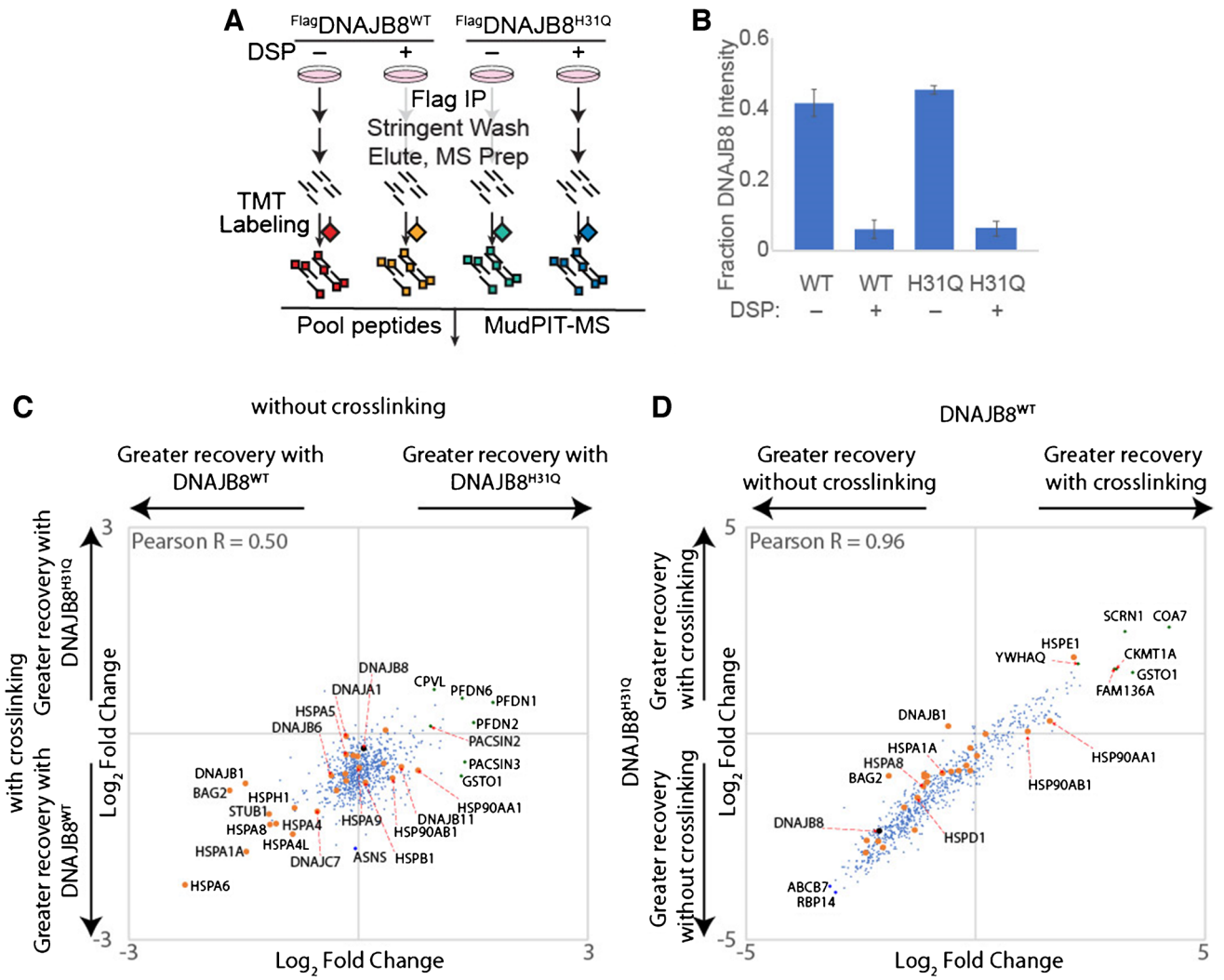

Fig. 3 Effect of J-domain integrity and cellular crosslinking on interactor recovery with DNAJB8. **A** Schematic of immunoprecipitation. **B** Recovery of DNAJB8 from each condition. Error bars represent standard deviation ($n=3$). All differences between conditions with different DSP treatment have $p<10^{-5}$ by post hoc Tukey's HSD after one-way ANOVA ($F=165$, $p=2\times10^{-7}$). **C**, **D** Relative association of interactors. Hsp70 chaperones and Hsp70-associated co-chaperones are shown in orange. Three biological replicates, comprising three LC–MS runs, were performed

Greater than 97% of the proteins identified were significant interactors from previous DNAJB8 immunoprecipitations (Fig. 1 and reference [20]). The J-domain mutation has only a modest effect on the interactor profile of DNAJB8 (Fig. 3C, Figure S3, and Table S2). As expected, cytosolic Hsp70 chaperones and associated co-chaperones have higher affinity for DNAJB8^{WT} than for DNAJB8^{H31Q}, reflecting the role of the J-domain in mediating their binding. This is true both in the presence and absence of crosslinking. By contrast, the ER and mitochondrial Hsp70s (HSPA5, HSPA9) have similar affinity for both DNAJB8s (Figure S3B and Table S2), suggesting that the J-domain is not mediating interactions with Hsp70s that DNAJB8 would not encounter during normal expression in the cell. The proteins with the strongest preference for DNAJB8^{H31Q} compared to DNAJB8^{WT} are the prefoldin β subunits (PFDN1: fold change = 3.4 ± 0.9 −DSP, PFDN2: fold changes = 2.8 ± 0.5 −DSP, PFDN6: fold changes = 2.6 ± 1.2 −DSP) (Figure S3B and Table S2). No such preference is found for components of the prominent prefoldin-associated complexes TRiC and RNA polymerase II, suggesting that the recognized prefoldin subunits are not actively engaged in those canonical prefoldin complexes [33]. Prefoldin subunits have also been found to act as holdase chaperones separately from their interactions with the TriC complex [34].

As expected, crosslinking sharply decreases DNAJB8 levels in the lysate as well as the recovered fraction (24 ± 5% recovery of DNAJB8^{WT}, 19 ± 7% recovery of DNAJB8^{H31Q}) (Fig. 3B). While this decrease could be due to DSP

modification of the lysine-rich Flag tag, the total protein concentration as measured by Bradford assay decreased by 48% ± 2% with DSP crosslinking, indicating that decreased protein solubility meaningfully contributes. Interestingly, crosslinking increases immunoprecipitation efficiency, perhaps by rendering any large DNAJB8-containing complexes insoluble (Figure S2D, E). The effect of crosslinking on interactor recovery is almost identical between the DNAJB8 baits, with a Pearson correlation of 0.96 between the two profiles (Fig. 3D**,** Figure S3**,** and Table S1). Crosslinking sharply decreases recovery of DNAJB8, and although it increases the recovery of interactors *relative to* DNAJB8, it is not enough to offset the decrease in DNAJB8 bait for most interactors. Exceptions include HSPE1 and a few 14–3-3 proteins, particularly 14–3-3θ/YWHAQ (fold change recovery = 4.8 ± 0.7% with DNAJB8^{WT}, fold change recovery = 3.2 ± 0.8% with DNAJB8^{H31Q}) (Figure S3B and Table S2). In summary, the primary consequence of DNAJB8 J-domain inactivation is to decrease association to Hsp70 family chaperones and co-chaperones, while crosslinking decreases DNAJB8 recovery so drastically as to eliminate any benefit from greater protein recovery.

Interactor recovery by DNAJB1 immunoprecipitation

Class B Hsp40s are distinguished by an N-terminal J-domain, a glycine/phenylalanine rich domain, two beta-barrel domains, and a C-terminal dimerization domain [15]. For cytosolic Class B Hsp40s, the first beta-barrel includes a weak Hsp70 binding site that is important for client transfer [35]. This class can be further divided into the two phylogenetic trees [36]. In one branch, DNAJB6 and DNAJB8 feature a unique serine/threonine rich region. This region is implicated in their remarkable ATP-independent holdase activity that substoichiometrically inhibits aggregation of some proteins [37–41], while still requiring Hsp70 to inhibit aggregation of other substrates [42, 43]. DNAJB6 and DNAJB8 also differ from other Class B Hsp40s in that they equilibrate between monomers and higher order oligomers, rather than the dimers and tetramers seen for other members of the class [44, 45], and lack the double beta barrel C-terminal domains present in canonical Hsp40 [46, 47]. It is not yet clear whether or how oligomerization generally impacts client binding and function, though the monomer appears to be the active form for at least some clients [40, 48–50]. The most abundant Hsp40 of the other branch is DNAJB1 which is homologous to yeast Sis1. DNAJB1 primarily forms dimers and monomers and has been found to demonstrate different substrate specificities in cellular and in vitro assays as opposed to DNAJB6 and DNAJB8 [37, 40, 51]. Given these structural differences and that DNAJB1 is one of the most studied human Hsp40s, we considered whether DNAJB1 could be similarly used to immunoprecipitate misfolded proteins.

We characterized the interaction networks of ^{Flag}DNAJB1^{WT} (in the absence of crosslinking) and ^{Flag}DNAJB1^{H32Q} (in the presence of crosslinking), to determine profiles of potential interactors (Fig. 4A, B**,** Figure S4A, and Table S3). While these conditions do not allow direct comparison to each other, they do allow comparisons to the equivalent DNAJB8 experiments of Fig. 2 and reference 8. The crosslinking concentration was based on optimization by TMT-AP-MS at varying concentrations of DNAJB1^{H32Q} (Figure S4B, C). Although median reporter ion intensities only change modestly with varying [DSP], there was a slight maximum at 0.25 mM DSP. We also found that extending the immunoprecipitation to 3 days increased DNAJB1 recovery (Figure S4D, E). DNAJB1^{WT} without crosslinking co-immunoprecipitates fewer proteins than DNAJB8^{WT} (Fig. 2), and the strongest interactors are almost entirely Hsp70s or their associated co-chaperones (Fig. 4A). 14/14 of the native interactors from Piette et al. [31] were found, though two (PYCR3, RPS10) did not show meaningful selectivity in our experiment between the presence or absence of DNAJB1^{WT}. 15/33 of Bioplex interactors [52, 53] (from HEK293) were identified, of which 4 (PYCR3, HDLBP, MAP2K2, and DIS3) did not show meaningful selectivity. These proteins participate in extensive interaction networks per Bioplex data, and they might lose affinity to DNAJB1 when these networks are disrupted by highly stringent RIPA buffer. As with DNAJB8^{WT}, common anti-Flag-binding contaminants are depleted in the ^{Flag}DNAJB1^{WT} immunoprecipitates. While DNAJB1^{H32Q} with crosslinking robustly recovers a larger proteome, the strongest interactions are still dominated by Hsp70 and Hsp70-associated chaperones. This is at first surprising, given the J-domain ablation. While the Hsp70 family proteins could be associating with DNAJB1^{H32Q} as clients, or as chaperones for misfolded DNAJB1^{H32Q}, the most likely explanation is that DNAJB1^{H32Q} is forming heterodimers with endogenous DNAJB1^{WT} or other endogenous J-domain proteins. Such heterodimers have been observed for most Class A and Class B DNAJ proteins [54, 55]. Still, DNAJB1^{H32Q} does interact with some proteins that were not recovered by either DNAJB8^{WT} or DNAJB8^{H31Q}, suggesting that it could potentially be useful for extending the space of proteins that are sampled by Hsp40 affinity profiling (Figure S5).

Influence of crosslinking and J-domain inactivation on DNAJB1 client binding

To better understand the role that the J-domain has in DNAJB1 interactor recovery, we directly compared interactor recovery for DNAJB1^{WT} vs. DNAJB1^{H32Q} in both the

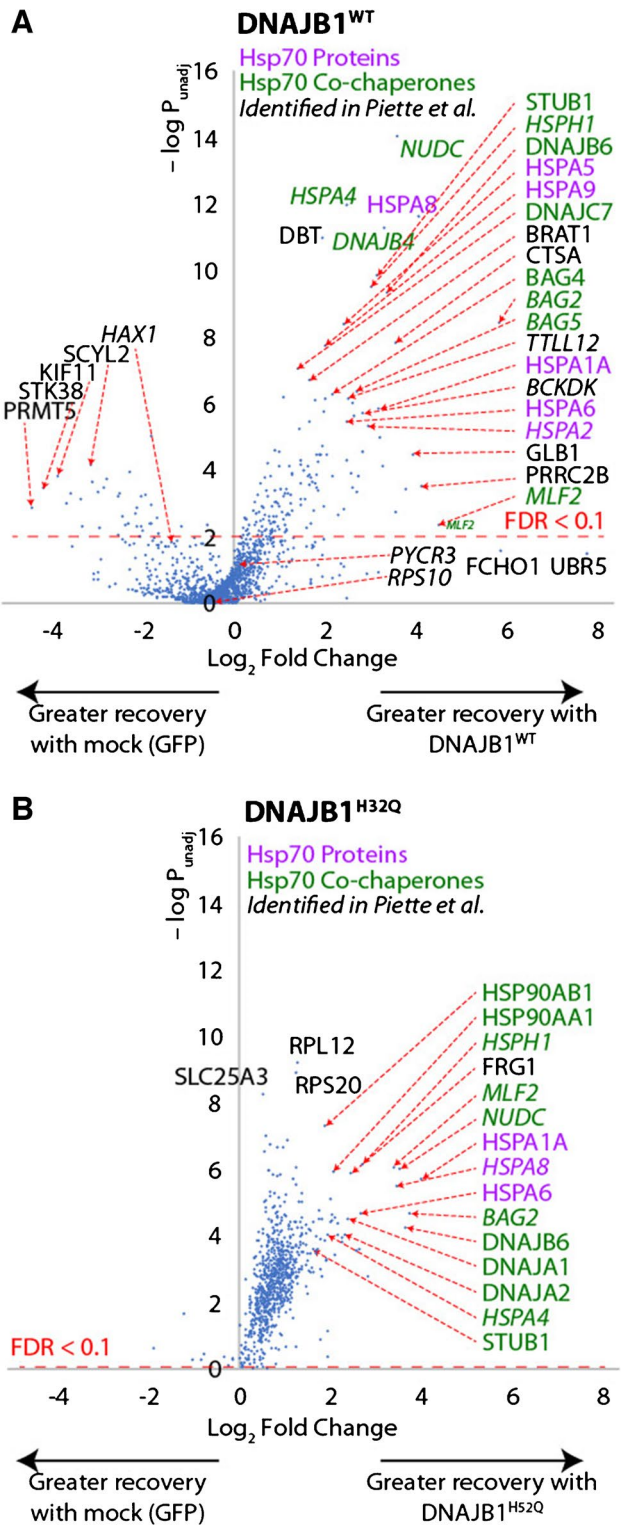

Fig. 4 **A** Proteins recovered by immunoprecipitation of ^{Flag}DNAJB1^{WT} without crosslinking (comparable to Fig. 2B) and **B** proteins recovered by immunoprecipitation of ^{Flag}DNAJB1^{H32Q} with crosslinking (comparable to ref. 8). Mock cells are transfected with eGFP. The experimental strategy is similar to that from Fig. 2A, except that the DNAJB1^{H32Q} AP-MS was preceded by cellular crosslinking with 250 µM DSP. Nine biological replicates, comprising three LC–MS runs, were performed for DNAJB1^{WT}, while six biological replicates, comprising two LC–MS runs, were performed for DNAJB1^{H32Q}. Hsp70 proteins are indicated in purple, Hsp70-associated co-chaperones are in green, and protein identified from Piette et al. [31] are italicized. The *p*-value cut-off corresponding to a 10% false discovery rate is indicated. The global false discovery rate for all proteins from Storey's modification of Benjamini–Hochberg analysis is 73% for DNAJB1^{WT} and 5.9% for DNAJB1^{H32Q}

absence and presence of crosslinking; this is similar to the experiment described in Fig. 3A for DNAJB8. In contrast to DNAJB8, there is far lower expression and hence recovery ($37 \pm 14\%$ –DSP, $25 \pm 10\% + $DSP) of DNAJB1^{H32Q} as opposed to DNAJB1^{WT} (Fig. 5A, Figure S6**A,** and Table S4). Crosslinking decreases the amount of DNAJB1 for both WT and H32Q ($62 \pm 9\%$ less recovered with crosslinking for DNAJB1^{WT}, $74 \pm 13\%$ less recovered with crosslinking for DNAJB1^{WT}), similarly to what was seen for DNAJB8. For both crosslinking and J-domain inactivation, however, the loss of bait is offset by a corresponding increase in protein recovery relative to DNAJB1 levels, such that overall interactor recoveries are similar across all four conditions (Fig. 5B, C and Figure S6B, C). Only half of the recovered proteins are high-confidence (with $q < 0.01$ from either experiment shown in Fig. 4) interactors of DNAJB1, most likely reflecting the lower overall protein recovery with DNAJB1. The distribution, however, is unaltered based on filtering for only the previously validated interactors (Figure S6D, S6E). As seen in Fig. 4B, DNAJB1^{H32Q} particularly enriches the inducible cytosolic Hsp70 HSPA1A (fold change $= 1.4 \pm 0.4 -$ DSP, $2.0 \pm 0.5 +$ DSP), despite lacking an active J-domain (Fig. 5B, Figure S6B, and Table S4). The WT protein, on the other hand, preferentially interacts with BCKDK (fold change $= 5.1 \pm 2.8 -$ DSP, $2.3 \pm 0.9 +$ DSP) and TTLL12 (fold change $= 3.3 \pm 2.2 -$ DSP, $2.6 \pm 1.3 +$ DSP) (Fig. 5B, Figure S6B, and Table S4). Crosslinking is necessary for recovery of 14–3-3 proteins and Hsp90s, but lowers recovery of BCKDK (Fig. 5C and Figure S6B). The low overall protein recovery made us consider that perhaps RIPA washing was responsible for removing interactors. Hence, we performed an identical set of experiments using a gentle lysis and wash buffer (0.1% Triton X-100 in TBS). Nearly identical results were obtained, except that overall protein identifications dropped to only 284 proteins (Figure S7). This decrease in protein recovery could be due to the low detergent buffer leading to less efficient lysis. While recovery in the DNAJB1^{WT} is unaffected, gentle washing increases protein recovery with DNAJB1^{H32Q} in the absence of crosslinking as opposed to in the presence of crosslinking. Overall, J-domain inactivation and crosslinking are, both individually and combined, effective approaches to increase interactor stoichiometry on DNAJB1. However, the low

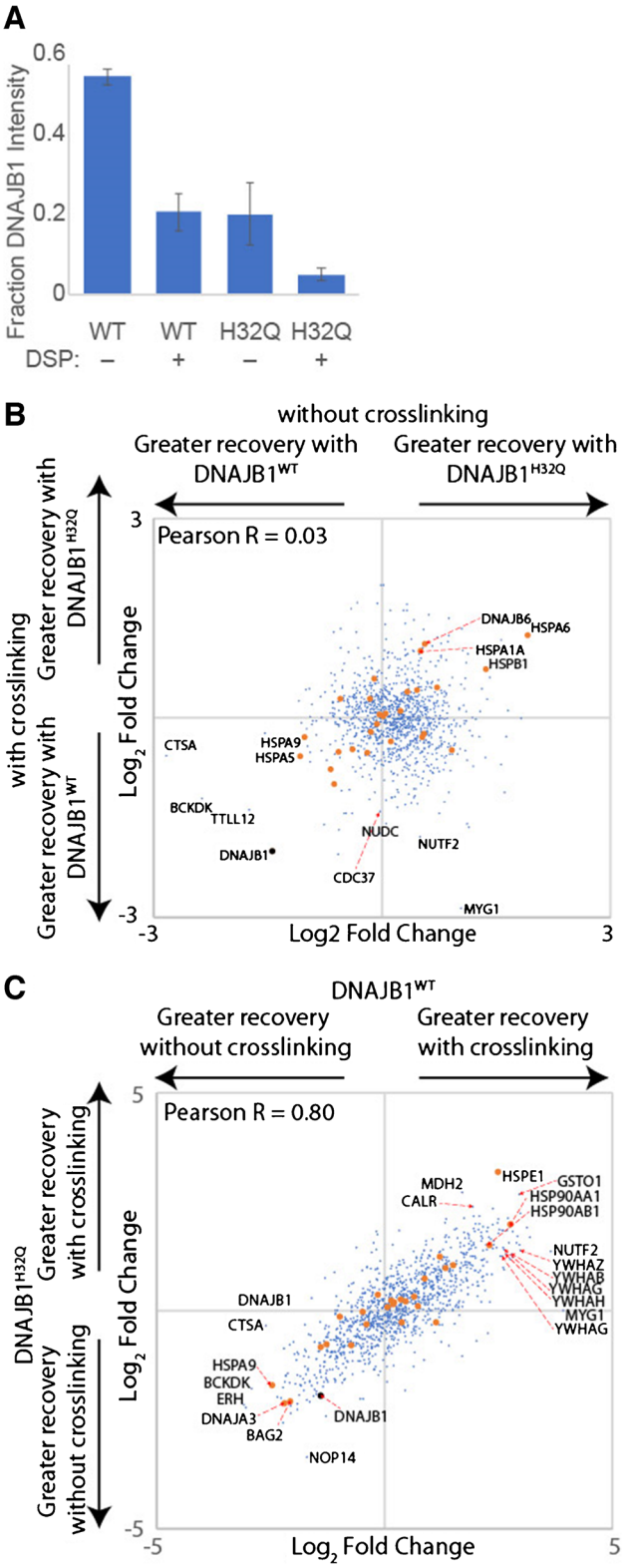

Fig. 5 Effect of J-domain integrity and cellular crosslinking on interactor recovery with DNAJB1. This data is from distinct experiments from those reported in Fig. 4. **A** Recovery of DNAJB1 from each condition. Error bars represent standard deviation ($n=3$). All differences between conditions have $p<0.02$ by post hoc Tukey's HSD after one-way ANOVA ($F=59$, $p=1\times10^{-5}$), except for WT + DSP and H32Q–DSP. **B**, **C** Relative association of interactors. Hsp70 chaperones and Hsp70-associated co-chaperones are shown in orange. Three biological replicates, comprising three LC–MS runs, were performed

recovery of DNAJB1 itself under both of these conditions offsets the greater interactor stoichiometry. This challenge would have to be overcome to make DNAJB1 a useful tool for separation of misfolded cellular proteins.

Cellular heat shock increases apparent affinity for DNAJB8^{H31Q} across the proteome

DNAJB8 demonstrates excellent client recovery, both with and without J-domain inactivation. The binding is strong even without crosslinking and following stringent washing, allowing elimination of most non-specific interactors. We considered how DNAJB8^{WT} and DNAJB8^{H31Q} compare with regard to their ability to identify changes in protein stability following a stress. We subjected ^{Flag}DNAJB8^{H31Q}-expressing HEK293T cells to mild heat stress for 30 min, followed by immediate lysis and anti-Flag immunoprecipitation (Fig. 6A). A condition with mock transfection (eGFP) under 47 °C heat shock was included to control for misfolding-induced affinity for beads. The short treatment was chosen to minimize transcriptional/translational remodeling of the cell due to induction of the heat shock response [56, 57]. The relative recovery of proteins was determined by MuDPIT LC–MS with isobaric TMT labeling, and integrated reporter ion ratios normalized to the amount of DNAJB8 bait. Proteins that showed less than twofold selectivity for the presence of DNAJB8 were excluded from further analysis (34 protein groups, dominated by the usual anti-Flag binding proteins discussed above), leaving 989 protein groups identified and quantified from all three runs. Consistent with the validated ability of DNAJB8^{H31Q} affinity to serve as a proxy for protein stability, we find that for about 80% of the proteome the Hsp40 affinity monotonically increases as the temperature increases from 37 to 45 °C, with plateauing or a slight drop-off at 47 °C (Fig. 6B,C, Figure S8A, B, and Table S5). For proteins that do not exhibit this trend, there is a tendency for Hsp40 affinity to increase from 37 to 43 °C, followed by a decrease in protein recovery. Although we did not collect sufficient data to estimate transition temperatures, we can estimate the sensitivity of Hsp40 affinity to temperature by taking the response factor (slope). We compared these slopes to published aggregation temperatures in HEK293T cells as determined by CETSA [58] and melting temperatures in HeLa cells determined from limited proteolysis [59] (Figure S8E). No correlation is found (643 protein groups found in both data sets, $R=0.0008$), as has been seen in other studies comparing relative destabilization using different methods [60]. We then performed a similar experiment with ^{Flag}DNAJB8^{WT}, now replacing the mock condition

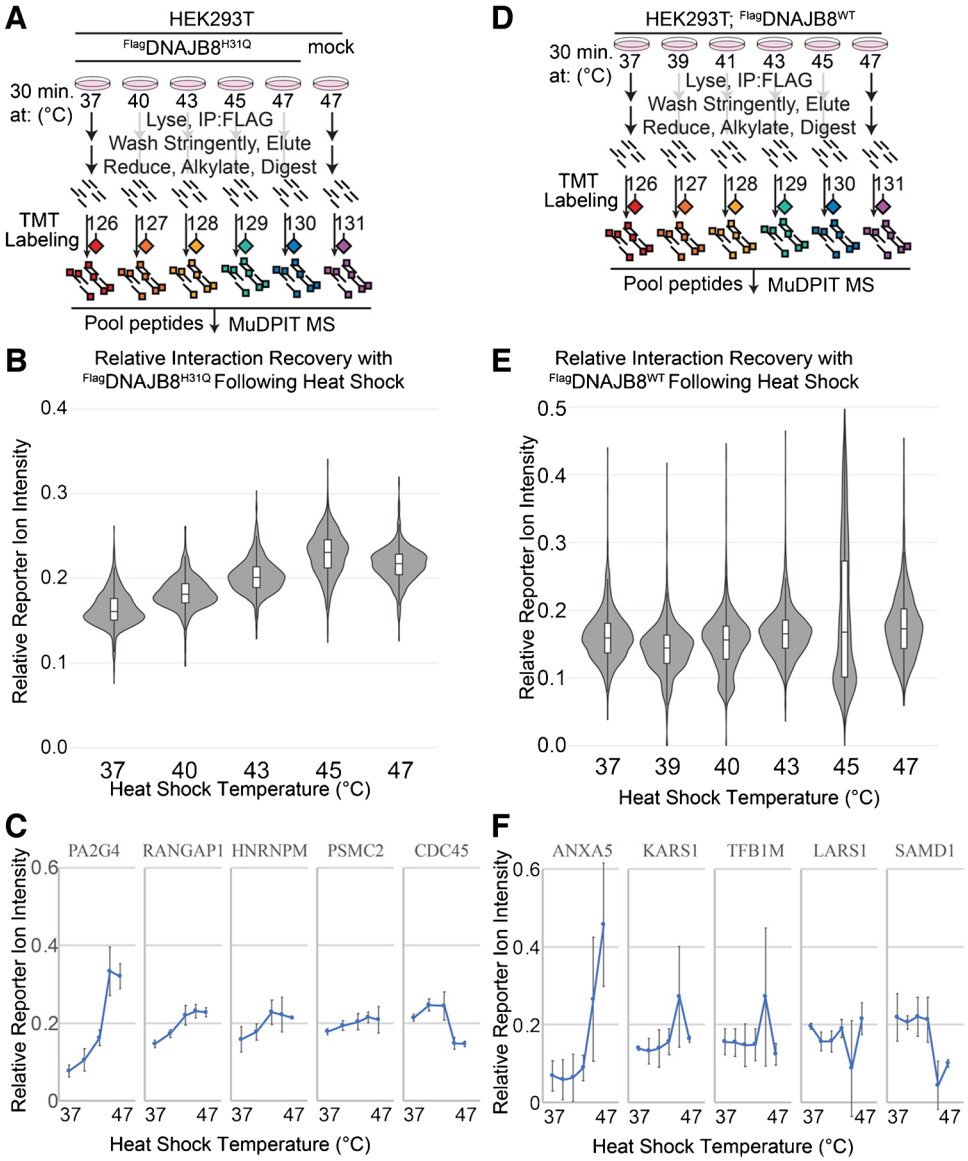

Fig. 6 **A** Schematic describing the experiment profiling DNAJB8^{H31Q} affinity following heat shock. **B** Violin and bar plots for all quantified interacting proteins ($n=989$). **C** Changes in reporter ion intensity for proteins with the highest, 25%, median, 75%, and lowest response with respect to temperature. Error bars represent standard deviation ($n=3$). **D** Schematic describing the experiment profiling DNAJB8^{WT} affinity following heat shock. **E** Violin and bar plots for all quantified interacting proteins ($n=1541$). **F** Changes in reporter ion intensity for proteins with the highest, 25%, median, 75%, and lowest response with respect to temperature. Error bars represent standard deviation ($n=3$)

with another temperature as little protein binding recovery had been seen in the mock condition (Fig. 6D). Surprisingly, we see only modest changes in DNAJB8^{WT} affinity with increasing temperature (Fig. 6E, F**,** Figure S8C, D, and Table S5). Although a few proteins show increased association, most show no change. Hence, while DNAJB8^{H31Q} is effective for recovering proteins that are destabilized by stress, DNAJB8^{WT} does not show the same capability.

Discussion

We previously demonstrated that DNAJB8^{H31Q} is effective for profiling the misfoldome in response to cellular stress [12], due to seemingly irreversible binding to misfolded proteins. DNAJB1 is one of the best studied Hsp40s due to its high concentration, promiscuous activity, selectivity for misfolded protein, and high similarity to yeast Sis1 [15, 35, 61, 62], leading us to consider whether DNAJB1 could be similarly used to recover misfolded proteins. We find that DNAJB1^{WT} preferentially associates with Hsp70 family members, pulling down a far less diverse proteome than DNAJB8 (Figure S5), consistent with its primarily ATP (and presumably Hsp70)-dependent biological function. While J-domain inactivation and crosslinking both help increase the relative protein load on DNAJB1, they decrease bait recovery so much that any benefit is offset. Crosslinkers vary in the functional groups that they target, in their solubility, and in the distance between targets. Expanding the range of crosslinkers used beyond DSP would be useful in case other crosslinkers provide improved performance. Furthermore, other Class B Hsp40

chaperones with substantial ATP-independent activity such as DNAJB6 or DNAJB2a might also serve as factors to expand the client profile accessible through DNAJB8^{H31Q}. It is important to stress that there is no reason to believe that the proteins recognized through this AP-MS assay reflect *native* cellular clients of Hsp40's. Rather, many of the interactions, such as those to mitochondrial and secretory proteins, are taking place post-lytically.

Given that both DNAJB8^{WT} and DNAJB8^{H31Q} strongly bind a large proteome under *basal* conditions, we expected that heat shock would have a similar effect on protein affinity for both chaperones. Specifically, we expected that heat-induced misfolding would increase the affinity for most proteins for both forms of DNAJB8. This was not the case, as heat shock increases client protein binding to DNAJB8^{H31Q} and not to DNAJB8^{WT} (Fig. 6). Rather, removing J-domain activity is necessary, in this context, to profile changes in protein stability with DNAJB8. The lack of increased client affinity for DNAJB8^{WT}, as opposed to DNAJB8^{H31Q}, could be due to the enhanced proteostasis activity following stress. If heat shock increases levels of Hsp70 or increases the activity of Hsp70, then even if client affinity for DNAJB^{WT} increases, so will the rate of hand-off to Hsp70. In this case, the steady state association of client proteins to DNAJB8^{WT} will only modestly change. This effect could even be aggravated by the active chaperoning of these client proteins, if Hsp70 is assisting in their refolding or degradation that will lower the overall misfolded protein load. By contrast, DNAJB8^{H31Q} is unable to hand substrates off to Hsp70. In that case, increased client affinity will not be balanced by a change in hand-off to Hsp70, leading to increased binding with the newly misfolded proteins during heat shock, as we observed.

One interesting unaddressed question is the role of DNAJB8 oligomerization. DNAJB8 and the structurally similar DNAJB6 form a distribution of oligomeric, dimeric, and monomeric stables, while DNAJB1 forms dimers [38, 48, 49]. The sluggish and non-first-order immunoprecipitation kinetics of ^{Flag}DNAJB8^{H31Q} (Figure S2F) suggest a heterogeneous population, such as would be found if immunoprecipitated DNAJB8 is primary in large structures. These are reminiscent of the large client-chaperone co-aggregates that we previously observed for secreted, but not cellular, DNAJB11 [63], despite its intracellular activity as a tetramer [44]. While it is tempting to infer that the strong binding of DNAJB8 to proteins is due to the avidity that comes with oligomerization, this model contrasts with the evidence so far that DNAJB8 primarily recognizes proteins as a monomer or dimer [49, 50].

The biophysics of the proteostasis network are complex, and the proteostasis of each protein is going to rely on a unique complement of proteostasis factors [64]. Under the conditions that we have used this assay, it has been successful at identifying proteins that are destabilized (or stabilized) by damage or direct binding subsequent to several disparate stresses [12–14]. However, this essentially chemoproteomic method does not report on how the proteostasis network of these proteins is changing or what factors make a client appropriate for DNAJB8 affinity profiling. Measuring affinity to other chaperones (including the wide diversity of Class C J-domain proteins) might allow us to profile a distinct client space, though the necessity that these chaperones bind misfolding proteins strongly enough to differentiate them from non-specific interactors will be the primary challenge in extending this assay to other chaperones.

In summary, DNAJB1 and DNAJB8 have been evaluated for their ability to profile proteins as part of an Hsp40 affinity assay. We find that DNAJB8^{H31Q} without crosslinking is the most effective approach and demonstrate that mild heat shock leads to generally monotonic increased affinity of clients with DNAJB8^{H31Q}.

Supplementary Information The online version contains supplementary material available at https://doi.org/10.1007/s00216-024-05362-1.

Acknowledgements eGFP.pDEST30 plasmid was generously shared by R.L. Wiseman.

Author contribution M.M.: Investigation, formal analysis, methodology, writing—original draft preparation. GQ: Investigation, formal analysis. LM: Investigation, methodology. JM: Investigation. CH: Investigation. JG: Conceptualization; formal analysis; project administration; supervision; visualization; writing, original draft preparation; writing, reviewing and editing.

Funding This work was supported by a Society of Analytical Chemists of Pittsburgh Starter Grant (J.C.G.) and the University of California, Riverside.

Data availability The mass spectrometry proteomics data and associated results files have been deposited to the ProteomeXchange Consortium via the PRIDE partner repository with the dataset identifier PXD030633.

Declarations

Conflict of interest The authors declare no competing interests.

References

1. Kim YE, Hipp MS, Bracher A, Hayer-Hartl M, Ulrich HF. Molecular chaperone functions in protein folding and proteostasis. Annu Rev Biochem. 2013;82(1):323–55.
2. Genereux JC. Profiling protein targets of cellular toxicant exposure. Mol Omics. 2023;19(3):191–204.
3. Kaur U, Meng H, Lui F, Ma R, Ogburn RN, Johnson JHR, et al. Proteome-wide structural biology: an emerging field for the structural analysis of proteins on the proteomic Scale. J Proteome Res. 2018;17(11):3614–27.
4. Bamberger C, Diedrich J, Martìnez-Bartholomé S, Yates JR. Cancer conformational landscape shapes tumorigenesis. J Proteome Res. 2022;21(4):1017–28.
5. Yin K, Tong M, Sun F, Wu R. Quantitative structural proteomics unveils the conformational changes of proteins under the endoplasmic reticulum stress. Anal Chem. 2022;94(38):13250–60.
6. Chavez JD, Wippel HH, Tang X, Keller A, Bruce JE. In-cell labeling and mass spectrometry for systems-level structural biology. Chem Rev. 2022;122(8):7647–89.
7. Cox D, Ormsby AR, Reid GE, Hatters DM. Protein painting reveals pervasive remodeling of conserved proteostasis machinery in response to pharmacological stimuli. Npj Syst Biol Appl. 2022;8(1):46.
8. To P, Xia Y, Lee SO, Devlin T, Fleming KG, Fried SD. A proteome-wide map of chaperone-assisted protein refolding in a cytosol-like milieu. Proc Natl Acad Sci. 2022;119(48): e2210536119.
9. Cappelletti V, Hauser T, Piazza I, Pepelnjak M, Malinovska L, Fuhrer T, et al. Dynamic 3D proteomes reveal protein functional alterations at high resolution in situ. Cell. 2021;184(2):545-559.e22.
10. Taipale M, Krykbaeva I, Whitesell L, Santagata S, Zhang J, Liu Q, et al. Chaperones as thermodynamic sensors of drug-target interactions reveal kinase inhibitor specificities in living cells. Nat Biotechnol. 2013;31(7):630–7.
11. Truman AW, Kristjansdottir K, Wolfgeher D, Ricco N, Mayampurath A, Volchenboum SL, et al. Quantitative proteomics of the yeast Hsp70/Hsp90 interactomes during DNA damage reveal chaperone-dependent regulation of ribonucleotide reductase. J Proteomics. 2015;112:285–300.
12. Quanrud GM, Montoya MR, Mei L, Awad MR, Genereux JC. Hsp40 affinity to identify proteins destabilized by cellular toxicant exposure. Anal Chem. 2021;93(50):16940–6.
13. Quanrud GM, Lyu Z, Balamurugan SV, Canizal C, Wu HT, Genereux JC. Cellular exposure to chloroacetanilide herbicides induces distinct protein destabilization profiles. ACS Chem Biol. 2023;18(7):1661–76.
14. Quanrud G, Abernathy M, Lyu Z, Ying S, Genereux J. Hsp40 affinity profiling reveals protein destabilization profiles following cellular manganese and vanadate exposure [Internet]. ChemRxiv; 2023 [cited 2023 Sep 29]. Available from: https://chemrxiv.org/engage/chemrxiv/article-details/6514b613ade1178b243eafc8
15. Kampinga HH, Craig EA. The HSP70 chaperone machinery: J proteins as drivers of functional specificity (vol 11, pg 579, 2010). Nat Rev Mol Cell Biol [Internet]. 2010 Oct;11(10). Available from: <Go to ISI>://WOS:000282152800018
16. Craig EA, Marszalek J. How do J-proteins get Hsp70 to do so many different things? Trends Biochem Sci. 2017;42(5):355–68.
17. Jin Y, Awad W, Petrova K, Hendershot LM. Regulated release of ERdj3 from unfolded proteins by BiP. EMBO J. 2008;27(21):2873–82.
18. Petrova K, Oyadomari S, Hendershot LM, Ron D. Regulated association of misfolded endoplasmic reticulum lumenal proteins with P58/DNAJc3. EMBO J. 2008;27(21):2862–72.
19. Klock HE, Lesley SA. The polymerase incomplete primer extension (PIPE) method applied to high-throughput cloning and site-directed mutagenesis. Methods Mol Biol. 2009;498:91–103.
20. Mei L, Montoya MR, Quanrud GM, Tran M, Villa-Sharma A, Huang M, et al. Bait correlation improves interactor identification by tandem mass tag-affinity purification-mass spectrometry. J Proteome Res. 2020;19(4):1565–73.
21. Shoulders MD, Ryno LM, Genereux JC, Moresco JJ, Tu PG, Wu C, et al. Stress-independent activation of XBP1s and/or ATF6 reveals three functionally diverse ER proteostasis environments. Cell Rep. 2013;3(4):1279–92.
22. Plate L, Rius B, Nguyen B, Genereux JC, Kelly JW, Wiseman RL. Quantitative interactome proteomics reveals a molecular Basis for ATF6-dependent regulation of a destabilized amyloidogenic protein. Cell Chem Biol. 2019;26(7):913-925.e4.
23. Washburn MP, Wolters D, Yates JR. Large-scale analysis of the yeast proteome by multidimensional protein identification technology. Nat Biotechnol. 2001;19(3):242–7.
24. Zecha J, Satpathy S, Kanashova T, Avanessian SC, Kane MH, Clauser KR, et al. TMT labeling for the masses: a robust and cost-efficient, in-solution labeling approach. Mol Cell Proteomics. 2019;18(7):1468–78.
25. Kong AT, Leprevost FV, Avtonomov DM, Mellacheruvu D, Nesvizhskii AI. MSFragger: ultrafast and comprehensive peptide identification in mass spectrometry–based proteomics. Nat Methods. 2017;14(5):513–20.
26. Hsieh EJ, Hoopmann MR, MacLean B, MacCoss MJ. Comparison of database search strategies for high precursor mass accuracy MS/MS data. J Proteome Res. 2010;9(2):1138–43.
27. Storey JD, Tibshirani R. Statistical significance for genomewide studies. Proc Natl Acad Sci U S A. 2003;100(16):9440–5.
28. Yekutieli D, Benjamini Y. Resampling-based false discovery rate controlling multiple test procedures for correlated test statistics. J Stat Plan Inference. 1999;82(1–2):171–96.
29. Mellacheruvu D, Wright Z, Couzens AL, Lambert JP, St-Denis NA, Li T, et al. The CRAPome: a contaminant repository for affinity purification-mass spectrometry data. Nat Methods. 2013;10(8):730–6.
30. Nishioka K, Reinberg D. Methods and tips for the purification of human histone methyltransferases. Methods San Diego Calif. 2003;31(1):49–58.
31. Piette BL, Alerasool N, Lin ZY, Lacoste J, Lam MHY, Qian WW, et al. Comprehensive interactome profiling of the human Hsp70 network highlights functional differentiation of J domains. Mol Cell. 2021;81(12):2549-2565.e8.
32. Smith AL, Friedman DB, Yu H, Carnahan RH, Reynolds AB. ReCLIP (reversible cross-link immuno-precipitation): an efficient method for interrogation of labile protein complexes. Jin DY, editor. PLoS ONE. 2011;6(1):e16206.
33. Gestaut D, Roh SH, Ma B, Pintilie G, Joachimiak LA, Leitner A, et al. The chaperonin TRiC/CCT associates with prefoldin through a conserved electrostatic interface essential for cellular proteostasis. Cell. 2019;177(3):751-765.e15.
34. Tahmaz I, ShahmoradiGhahe S, Topf U. Prefoldin function in cellular protein homeostasis and human diseases. Front Cell Dev Biol. 2022;9: 816214.
35. Faust O, Abayev-Avraham M, Wentink AS, Maurer M, Nillegoda NB, London N, et al. HSP40 proteins use class-specific regulation to drive HSP70 functional diversity. Nature. 2020;587(7834):489–94.
36. Hageman J, Kampinga HH. Computational analysis of the human HSPH/HSPA/DNAJ family and cloning of a human HSPH/HSPA/DNAJ expression library. Cell Stress Chaperones. 2009;14(1):1–21.
37. Hageman J, Rujano MA, van Waarde MAWH, Kakkar V, Dirks RP, Govorukhina N, et al. A DNAJB chaperone subfamily with

HDAC-dependent activities suppresses toxic protein aggregation. Mol Cell. 2010;37(3):355–69.
38. Gillis J, Schipper-Krom S, Juenemann K, Gruber A, Coolen S, van den Nieuwendijk R, et al. The DNAJB6 and DNAJB8 protein chaperones prevent intracellular aggregation of polyglutamine peptides. J Biol Chem. 2013;288(24):17225–37.
39. Rozales K, Younis A, Saida N, Meller A, Goldman H, Kellerman L, et al. Differential roles for DNAJ isoforms in HTT-polyQ and FUS aggregation modulation revealed by chaperone screens. Nat Commun. 2022;13(1):516.
40. Månsson C, Kakkar V, Monsellier E, Sourigues Y, Härmark J, Kampinga HH, et al. DNAJB6 is a peptide-binding chaperone which can suppress amyloid fibrillation of polyglutamine peptides at substoichiometric molar ratios. Cell Stress Chaperones. 2014;19(2):227–39.
41. Abayev-Avraham M, Salzberg Y, Gliksberg D, Oren-Suissa M, Rosenzweig R. DNAJB6 mutants display toxic gain of function through unregulated interaction with Hsp70 chaperones. Nat Commun. 2023;14(1):7066.
42. McMahon S, Bergink S, Kampinga HH, Ecroyd H. DNAJB chaperones suppress destabilised protein aggregation via a region distinct from that used to inhibit amyloidogenesis. J Cell Sci. 2021;134(7):jcs255596.
43. Ryder BD, Matlahov I, Bali S, Vaquer-Alicea J, van der Wel PCA, Joachimiak LA. Regulatory inter-domain interactions influence Hsp70 recruitment to the DnaJB8 chaperone. Nat Commun. 2021;12(1):946.
44. Chen KC, Qu S, Chowdhury S, Noxon IC, Schonhoft JD, Plate L, et al. The endoplasmic reticulum HSP40 co-chaperone ERdj3/DNAJB11 assembles and functions as a tetramer. EMBO J. 2017;36(15):2296–309.
45. Stirling PC, Bakhoum SF, Feigl AB, Leroux MR. Convergent evolution of clamp-like binding sites in diverse chaperones. Nat Struct Mol Biol. 2006;13(10):865–70.
46. Karamanos TK, Tugarinov V, Clore GM. Unraveling the structure and dynamics of the human DNAJB6b chaperone by NMR reveals insights into Hsp40-mediated proteostasis. Proc Natl Acad Sci. 2019;116(43):21529–38.
47. Karamanos TK, Tugarinov V, Clore GM. An S/T motif controls reversible oligomerization of the Hsp40 chaperone DNAJB6b through subtle reorganization of a β sheet backbone. Proc Natl Acad Sci. 2020;117(48):30441–50.
48. Söderberg CAG, Månsson C, Bernfur K, Rutsdottir G, Härmark J, Rajan S, et al. Structural modelling of the DNAJB6 oligomeric chaperone shows a peptide-binding cleft lined with conserved S/T-residues at the dimer interface. Sci Rep. 2018;8(1):5199.
49. Ryder BD, Ustyantseva E, Boyer DR, Mendoza-Oliva A, Kuska MI, Wydorski PM, et al. DNAJB8 oligomerization is mediated by an aromatic-rich motif that is dispensable for substrate activity. Struct Lond Engl 1993. 2024;S0969–2126(24)00055–8.
50. Carlsson A, Axell E, Emanuelsson C, Olsson U, Linse S. The ability of DNAJB6b to suppress amyloid formation depends on the chaperone aggregation state. ACS Chem Neurosci. 2024;15(9):732–1737.
51. Ayala Mariscal SM, Pigazzini ML, Richter Y, Özel M, Grothaus IL, Protze J, et al. Identification of a HTT-specific binding motif in DNAJB1 essential for suppression and disaggregation of HTT. Nat Commun. 2022;13(1):4692.
52. Huttlin EL, Bruckner RJ, Navarrete-Perea J, Cannon JR, Baltier K, Gebreab F, et al. Dual proteome-scale networks reveal cell-specific remodeling of the human interactome. Cell. 2021;184(11):3022-3040.e28.
53. Schweppe DK, Huttlin EL, Harper JW, Gygi SP. BioPlex display: an interactive suite for large-scale AP–MS protein–protein interaction data. J Proteome Res. 2018;17(1):722–6.
54. Otero JH, Lizák B, Feige MJ, Hendershot LM. Dissection of structural and functional requirements that underlie the interaction of ERdj3 protein with substrates in the endoplasmic reticulum. J Biol Chem. 2014;289(40):27504–12.
55. Rosenzweig R, Nillegoda NB, Mayer MP, Bukau B. The Hsp70 chaperone network. Nat Rev Mol Cell Biol. 2019;20(11):665–80.
56. Moloney TC, Hoban DB, Barry FP, Howard L, Dowd E. Kinetics of thermally induced heat shock protein 27 and 70 expression by bone marrow-derived mesenchymal stem cells: Heat Shock Protein Expression in MSC. Protein Sci. 2012;21(6):904–9.
57. Diller KR. Stress protein expression kinetics. Annu Rev Biomed Eng. 2006;8(1):403–24.
58. Jarzab A, Kurzawa N, Hopf T, Moerch M, Zecha J, Leijten N, et al. Meltome atlas—thermal proteome stability across the tree of life. Nat Methods. 2020;17(5):495–503.
59 Leuenberger P, Ganscha S, Kahraman A, Cappelletti V, Boersema PJ, von Mering C, et al. Cell-wide analysis of protein thermal unfolding reveals determinants of thermostability. Science. 2017;355(6327):eaai7825.
60. Cox J, Hein MY, Luber CA, Paron I, Nagaraj N, Mann M. Accurate proteome-wide label-free quantification by delayed normalization and maximal peptide ratio extraction. Termed MaxLFQ Mol Cell Proteomics. 2014;13(9):2513–26.
61 Yu HY, Ziegelhoffer T, Craig EA. Functionality of class A and class B J-protein co-chaperones with Hsp70. FEBS Lett. 2015;589(19PartB):2825–30.
62 Irwin R, Faust O, Petrovic I, Wolf SG, Hofmann H, Rosenzweig R. Hsp40s play complementary roles in the prevention of tau amyloid formation. eLife. 2021;10:e69601.
63. Genereux JC, Qu S, Zhou M, Ryno LM, Wang S, Shoulders MD, et al. Unfolded protein response-induced ERdj3 secretion links ER stress to extracellular proteostasis. EMBO J. 2015;34(1):4–19.
64. Powers ET, Gierasch LM. The proteome folding problem and cellular proteostasis. J Mol Biol. 2021;433(20): 167197.